Lateral cerebellum is preferentially sensitive to high sonic hedgehog signaling and medulloblastoma formation

I-Li Tan[a,b,1], Alexandre Wojcinski[a,1], Harikrishna Rallapalli[c], Zhimin Lao[a], Reeti M. Sanghrajka[a,b], Daniel Stephen[a], Eugenia Volkova[c], Andrey Korshunov[d,e], Marc Remke[f], Michael D. Taylor[e,g], Daniel H. Turnbull[c], and Alexandra L. Joyner[a,b,2]

[a]Developmental Biology Program, Sloan Kettering Institute, New York, NY 10065; [b]Biochemistry, Cell, and Molecular Biology Program, Weill Graduate School of Medical Sciences of Cornell University, New York, NY 10065; [c]Skirball Institute of Biomolecular Medicine, Department of Radiology, New York University School of Medicine, New York, NY 10016; [d]Clinical Cooperation Unit Neuropathology, German Cancer Research Center, University Hospital, 69120 Heidelberg, Germany; [e]Department of Neuropathology, University Hospital, 69120 Heidelberg, Germany; [f]The Arthur and Sonia Labatt Brain Tumour Research Centre, Hospital for Sick Children, Toronto, ON M5G 0A4, Canada; and [g]Division of Neurosurgery, Department of Surgery, University of Toronto, Toronto, ON M5S 1A1, Canada

Edited by Matthew P. Scott, Carnegie Institution for Science, Washington, DC, and approved February 16, 2018 (received for review October 18, 2017)

The main cell of origin of the Sonic hedgehog (SHH) subgroup of medulloblastoma (MB) is granule cell precursors (GCPs), a SHH-dependent transient amplifying population in the developing cerebellum. SHH-MBs can be further subdivided based on molecular and clinical parameters, as well as location because SHH-MBs occur preferentially in the lateral cerebellum (hemispheres). Our analysis of adult patient data suggests that tumors with Smoothened (*SMO*) mutations form more specifically in the hemispheres than those with Patched 1 (*PTCH1*) mutations. Using sporadic mouse models of SHH-MB with the two mutations commonly seen in adult MB, constitutive activation of *Smo* (*SmoM2*) or loss-of-*Ptch1*, we found that regardless of timing of induction or type of mutation, tumors developed primarily in the hemispheres, with *SmoM2*-mutants indeed showing a stronger specificity. We further uncovered that GCPs in the hemispheres are more susceptible to high-level SHH signaling compared with GCPs in the medial cerebellum (vermis), as more *SmoM2* or *Ptch1*-mutant hemisphere cells remain undifferentiated and show increased tumorigenicity when transplanted. Finally, we identified location-specific GCP gene-expression profiles, and found that deletion of the genes most highly expressed in the hemispheres (*Nr2f2*) or vermis (Engrailed1) showed opposing effects on GCP differentiation. Our studies thus provide insights into intrinsic differences within GCPs that impact on SHH-MB progression.

granule cell precursors | Nr2f2 | En1 | cerebellar hemispheres | MRI

Medulloblastoma (MB) is the most common malignant pediatric brain cancer and comprises four major subgroups [WNT, Sonic hedgehog (SHH), group 3, and group 4], with further subdivisions proposed to explain the diverse genetics, cells of origin, and clinical presentations of the disease (1–5). Aggressive treatment protocols used to treat young MB patients impact on central nervous system development and lead to long-term neurocognitive sequelae (6). Thus, it is critical to gain new insights into the biology of each subgroup to strengthen stratification and enable development of targeted therapies.

SHH-MB (~30% of all MBs) is the most diverse subgroup in terms of histology and age of presentation. Proliferation of granule cell precursors (GCPs) that give rise to SHH-MB is regulated by HH signaling during the third trimester to the first few months of life in human, and from approximately embryonic day (E) 17 to postnatal day (P) 16 in mice (7–12). Nearly 90% of SHH-MB samples have a mutation in four genes that lead to HH pathway activation (2): loss-of-function mutations in two genes that inhibit the HH pathway [Patched 1 (*PTCH1*) and *SUFU*], activating mutations in Smoothened (*SMO*), and *TP53* loss associated with amplification of *GLI2* or *NMYC* that act downstream of SHH. Interestingly, *SUFU* mutations are mainly seen in infants (≤3 y old), *TP53* mutations in children (4–17 y old), and *SMO* in adults (≥18 y old), whereas *PTCH1* mutations are seen across ages (2, 13). Additional *TERT* mutations are seen in most adult tumors (14). SHH-MBs are more often located in the lateral cerebellum (hemispheres, H) whereas the other MB subgroups are mainly found in the midline (vermis, V) (15, 16). Notably, adult SHH-MBs in particular preferentially arise in the H compared with infant SHH-MBs (17). One limited study in two mouse models also indicated preferential occurrence of SHH-MB in the H (18). The underlying reason why driver mutations and tumor locations are associated with particular SHH-MB patient age groups has not been addressed experientially.

The H and V of the cerebellum have different morphologies and numbers of lobules, as well as different functions. As different genetic programs in the two locations could account for the distinct foliation patterns, we hypothesized that SHH-MBs arise preferentially in the H because the location of GCPs

Significance

Cerebellar tumor medulloblastoma (MB) is no longer considered a single disease as it has been separated into four subgroups with further subdivisions based on genomic and clinical data. Mechanistic understandings of the stratification within subgroups should allow for better-targeted treatments. We redefined the main cell of origin by showing that granule cell precursors (GCPs) are heterogeneous with molecularly distinct populations based on their location. As a consequence, GCPs respond differentially to two driver mutations, and a subset of GCPs is more susceptible to Sonic hedgehog (SHH) pathway elevation and forms tumors more readily. These results provide insights into the preferential location of human SHH-MBs in the lateral cerebellum and the cellular and genetic factors influencing SHH-MB progression.

Author contributions: I.-L.T., A.W., D.H.T., and A.L.J. designed research; I.-L.T., A.W., H.R., Z.L., R.M.S., D.S., and E.V. performed research; H.R., E.V., A.K., and D.H.T. contributed new reagents/analytic tools; I.-L.T., A.W., H.R., Z.L., R.M.S., E.V., M.R., M.D.T., D.H.T., and A.L.J. analyzed data; and I.-L.T., A.W., H.R., D.H.T., and A.L.J. wrote the paper.

The authors declare no conflict of interest.

This article is a PNAS Direct Submission.

Data deposition: The data reported in this paper have been deposited in the Gene Expression Omnibus (GEO) database, https://www.ncbi.nlm.nih.gov/geo (accession no. GSE110932).

[1]I.-L.T. and A.W. contributed equally to this work.

[2]To whom correspondence should be addressed. Email: joynera@mskcc.org.

This article contains supporting information online at www.pnas.org/lookup/suppl/doi:10.1073/pnas.1717815115/-/DCSupplemental.

Published online March 12, 2018.

dictates their susceptibility to driver mutations in the SHH pathway. By expressing a constitutively active form of *SMO* (*SmoM2*) or inducing a *Ptch1* loss-of-function mutation in a mosaic fashion in GCPs at P2, we found that mutant GCPs located in H have a lower probability of differentiating than those in V, and that *SmoM2* is a stronger driver of this phenotype. Longitudinal MRI imaging revealed that all *SmoM2*-mutant tumors develop in the H, and transplantation of *SmoM2*-mutant cells revealed a higher tumor-forming ability of hemispheric GCPs/lesions. Using a genomic approach, we identified two location-specific GCP genes that have predictable effects on GCP differentiation. Thus, GCPs can be divided into at least two subpopulations based on their location with distinct sensitivities to high HH signaling and tumorigenicity. Our studies represent an approach for stratifying SHH-MBs and identifying candidate genes that mediate tumor formation.

Results

Initiating Mutation in Human Adult SHH-MB Appears to Influence Tumor Location. We analyzed data from 38 SHH-MB patients to test whether there is a correlation between mutation and location, because this was not previously addressed (Table S1). Consistent with previous reports, 58% (22 of 38) of the SHH-MBs were located in the H, with 50% (5 of 10) of infant, 54% (7 of 13) of childhood, and 67% (10 of 15) of adult tumors located in the H (Fig. 1*A*). Interestingly, 80% (4 of 5) of tumors with a *SMO* mutation, 59% (10 of 17) of tumors with a *PTCH1* mutation, and 67% (8 of 14) of tumors with a *TP53* mutation were located in the H. The two infant tumors with an *SUFU* mutation were both located in the V (Fig. 1*B*). Interestingly, in adults all of the *SMO*-mutant tumors (four of four) were located in the H, whereas 59% (five of nine) of the adult *PTCH*-mutant tumors formed in the H (Fig. 1*C*). In summary, we found that SHH-MB tumors with *PTCH1*, *TP53*,

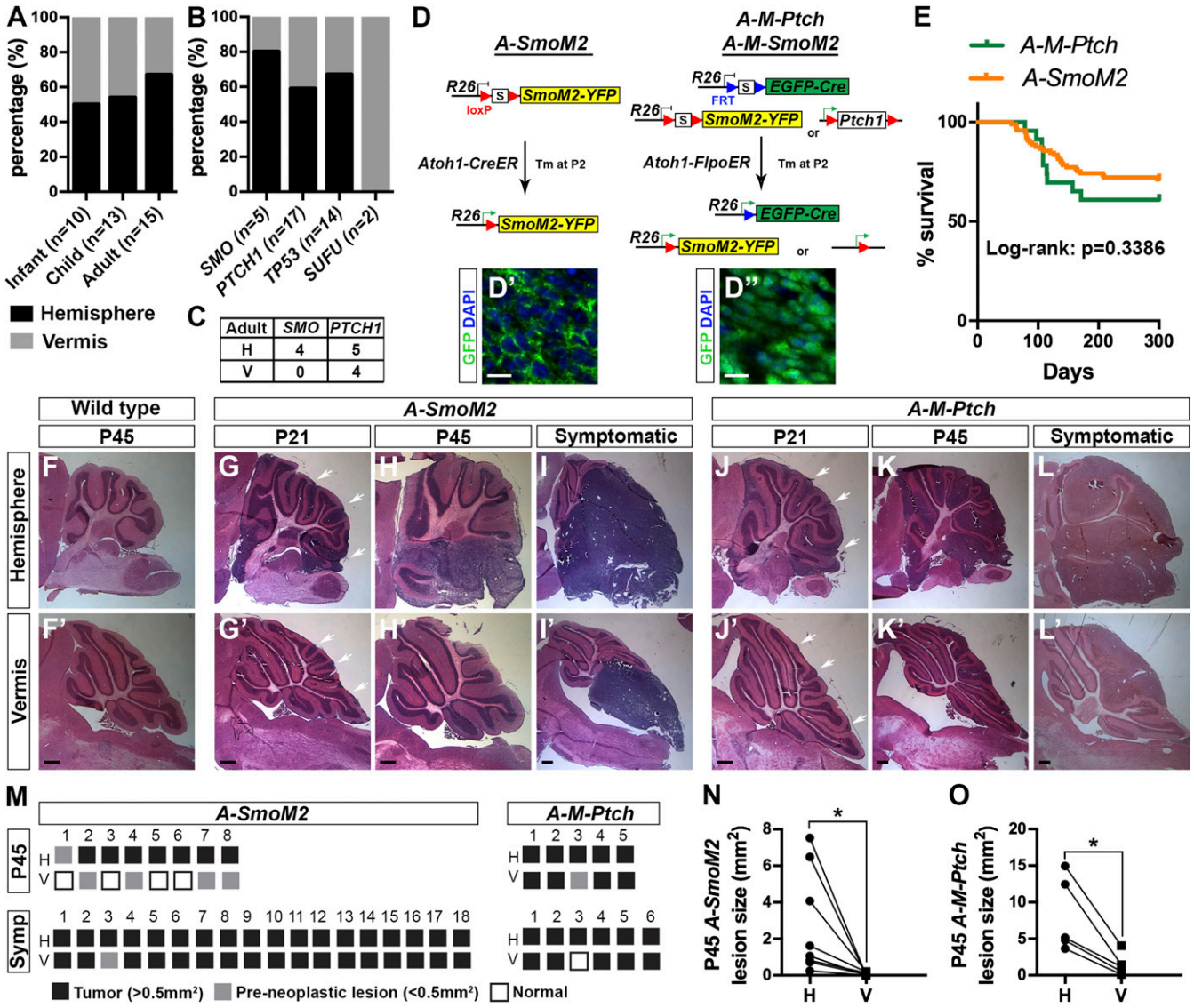

Fig. 1. Human and mouse SHH-MBs are preferentially located in the cerebellar H. (*A* and *B*) Percentage of tumors located in H and V from 38 SHH-MBs separated by patient age group (*A*) or mutation types (*B*). (*C*) Number of adult tumors located in H and V with *SMO* or *PTCH1* mutations (one-tailed χ^2 test, $P = 0.0545$). (*D*–*D*″) Schematic showing the three sporadic SHH-MB mouse models used. (Scale bars, 10 μm.) (*E*) Survival curves for two models. (*F*–*L*) H&E staining of sagittal sections in H and V (*F*′–*L*′) from mice of the indicated genotypes and ages. White arrows indicate lesions. (Scale bars, 500 μm.) (*M*) Schematic showing the presence of tumors or preneoplastic lesions in individual P45 and symptomatic *A-SmoM2* or *A-M-Ptch* mice. (*N* and *O*) Graphs showing the size of H and V lesions in P45 *A-SmoM2* ($n = 8$) (*N*) and *A-M-Ptch* ($n = 5$) (*O*) mice, with lines connecting data from each animal. Significance was determined using two-tailed Student's *t* test, $^*P < 0.05$. Statistics are provided in Table S2.

or *SMO* mutations preferentially form in the H, with an even higher correlation for adult tumors with *SMO* mutations.

Mouse Sporadic Postnatal Models of SHH-MB Preferentially Arise in the Cerebellar Hemispheres. Because adult SHH-MBs with *SMO* mutations appear to form more specifically in the H than those with *PTCH1*-mutations, we determined the location of tumors in mouse models with mutations in the same genes. A previous genomic study comparing multiple mouse MB models to their human counterparts suggested that mice expressing *SmoM2* or with loss-of-*Ptch1* mainly model adult SHH-MBs (13). To more closely model human tumors, we used inducible recombination approaches to express *SmoM2* (19) or delete *Ptch1* (20) in a small number of GCPs after birth to avoid modeling infant tumors (Fig. 1*D*). *Atoh1-CreER/+;R26*$^{LSL\text{-}SmoM2\text{-}YFP/+}$ mice (LSL, loxP-stop-loxP) were injected with a very low dose of Tamoxifen (Tm) at P2 (*A-SmoM2*) that induced recombination in ∼400 GCPs evenly scattered across the cerebellum that express membrane YFP (Fig. 1*D′* and Fig. S1). In the loss-of-*Ptch1* model, our FLP-inducible *R26*-based MASTR (mosaic analysis with spatial and temporal control of recombination) allele (21) was used to express eGFPcre in scattered GCPs (∼10,000 per cerebellum) and delete *Ptch1* (*Atoh1-FlpoER/+;R26*$^{MASTR/+}$*;Ptch1*$^{flox/flox}$ mice given a high dose of Tm at P2; *A-M-Ptch* model). Tm-induced mutant cells were identified by nuclear GFP signal (Fig. 1*D′′*). To directly compare *Ptch1* and *SmoM2* models, we also generated a small number of *A-M-SmoM2* mice and verified that they had a similar tumor progression profile as the simpler *A-SmoM2* model (Fig. S2 A–C).

In the *A-SmoM2* model, 29% (28 of 97) of mice showed symptoms of tumor burden with a median age of death of 114.5 d (range 56–297 d) (Fig. 1*E*). If only litters in which at least one mouse developed a tumor are included, because the very low dose of Tm used results in some inconsistency in tumor induction, then 56% (28 of 50) of mice developed tumors. In the *A-M-Ptch* model, 39% (9 of 23) of mice developed tumors with a median age of death of 108 d (range 78–171 d). In all models, preneoplastic lesions (defined as <0.5 mm^2) were detected at P21 throughout both the H and V, but the lesions appeared larger in the H (Fig. 1 *G–J*). Interestingly at P45, tumors (defined as >0.5 mm^2) in both *A-SmoM2* (n = 8) and *A-M-SmoM2* (n = 10) models were located only in the H (Fig. 1 *H* and *M* and Fig. S2D). In contrast, although the P45 tumors in the H were always larger than those in the V, most *A-M-Ptch* mice had tumors located in both locations (four of five) (Fig. 1 *K* and *O*). Thus, our results in the two mouse models at P45 correlate with the broader location of tumors in adult human *PTCH1* SHH-MBs compared with the H-specific location of *SMO* mutations.

By the time *A-SmoM2* mice became symptomatic, very large continuous tumors were seen that extended from the H to under the V (17 of 18) (Fig. 1 *I* and *M*). To confirm that *SmoM2*-tumors arose exclusively in the H, we utilized manganese-enhanced MRI (MEMRI) (22) to track tumor progression longitudinally in individual *A-SmoM2* mice (n = 21). The high tissue contrast images obtained with MEMRI allowed for detection of small lesions at ∼P21 (Fig. S3) (22) through to advanced tumors (Fig. 2*A*). We identified preneoplastic lesions across the whole cerebellum at 3 wk in all mice; however, only 14 of 21 mice had small tumors at ∼7 wk. Interestingly, the lesions that were present in the V at ∼3 wk could not be detected at ∼7 wk (Fig. 2*B*), consistent with our histological analysis of independent tumors (Fig. 1*H′*). Seven of 14 mice with tumors at ∼P45 progressed to have tumor symptoms from 11 to 13 wk and some advanced tumors grew from one H to the posterior midline after P45 (Fig. S4). The remaining 7 of 14 mice either had only minor tumor growth or the tumors regressed after P45. Our longitudinal imaging of tumor progression thus confirmed that *A-SmoM2* tumors specifically arose from the H.

Timing of Mutation Induction Does Not Change Tumor Location. We next asked whether the time when the mutation is induced affects tumor location, by giving a low dose of Tm to *A-SmoM2* mice at E14.5. Interestingly, at P21 all seven mice analyzed had lesions/small tumors in the H, whereas only four of seven had small lesions in the V (Fig. S5 A and D). At P45, all eight mice had larger tumors in the H than the V (Fig. S5 B and C), and all of the tumors in the V (five of eight mice) were continuous with the ones in the H, indicating that the tumors had initiated in the H. Thus, the timing of induction of the initiating mutation does not have a major effect on the location where *A-SmoM2* tumors form.

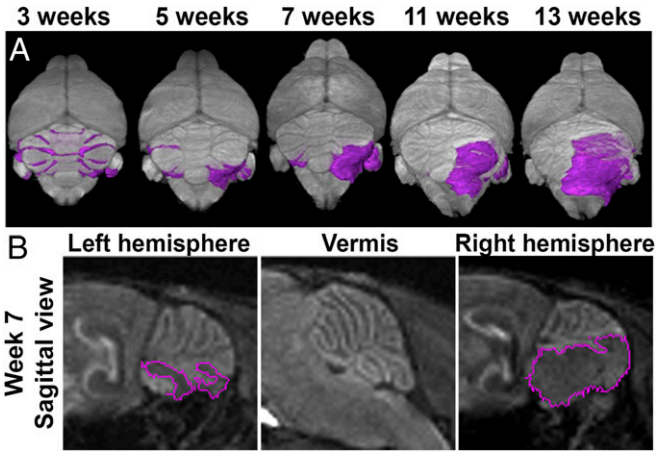

Fig. 2. MEMRI longitudinal imaging of *A-SmoM2* mice demonstrates tumors arise in the lateral cerebellum. (*A*) Representative 3D volume renderings of the brain (gray) and lesions/tumors (purple) from MEMRI longitudinal imaging of *A-SmoM2* mice at the indicated time points. (*B*) MEMRI sagittal views in left/right H and V in 7 wk *A-SmoM2* mice. Lesions/tumors are marked by purple lines.

Maintenance of GCPs in a Progenitor State by Hyperactivation of SHH Signaling Is More Pronounced in the H. The fact that SHH-MBs arise preferentially in a specific location led us to hypothesize that Atoh1$^+$ GCPs are not a homogeneous population, and that GCPs in the H are more susceptible to hyperactivation of the SHH pathway than those in the V. To test this hypothesis, we evaluated the percentage of undifferentiated nuclear GFP$^+$ GCPs [GFP$^+$ in the proliferating outer external granule cell layer (EGL)/total GFP$^+$ cells] and the proliferation index [GFP$^+$ EdU$^+$ (5-ethynyl-2-deoxyuridine) cells/GFP$^+$ in the outer EGL] in the H and V of P8 controls *A-M* (*Atoh1-FlpoER/+;R26*$^{MASTR/+}$) and *A-M-SmoM2* and *A-M-Ptch* mice given Tm at P2 (Fig. S6A). As expected, we observed a significantly higher percentage of undifferentiated GCPs in *A-M-SmoM2* and *A-M-Ptch* compared with control mice (Fig. S6B). Interestingly, more *SmoM2*-mutant GCPs remained in an undifferentiated state compared with *Ptch1*-mutant (Fig. S6B). Using a 1-h pulse of EdU to evaluate the proliferation index, we found that both *SmoM2*-mutant and *Ptch1*-mutant GCPs had a significant increase in the proliferation index compared with controls (Fig. S6C). Interestingly, when comparing between two locations within mice of each genotype, the H showed a significantly higher percentage of undifferentiated GCPs than the V in *SmoM2* and *Ptch1*-mutants, but there was no difference in the control mice (Fig. 3*A*). However, there was no difference in terms of the proliferation index between the H and V in the controls or mutants (Fig. 3*B*).

Correlating with the different rate of differentiation observed between the two mutants at P8, we found a higher percentage of P27$^+$ cells in *A-M-Ptch* lesions than in *A-M-SmoM2* lesions at P21 suggesting that the *SmoM2* mutation preferentially inhibits differentiation of GCPs compared with loss-of-*Ptch1* for a sustained time period (Fig. 3 *C–F* and Fig. S6 D–K). However, we observed no significant difference between the H and V in each model at this age (Fig. 3*G*). Notably, the higher percentage of postmitotic mutant cells in *A-M-Ptch* mice likely accounted for a larger cerebellum size in the mutants compared with *A-M-SmoM2* mice (Fig. S6 E and G).

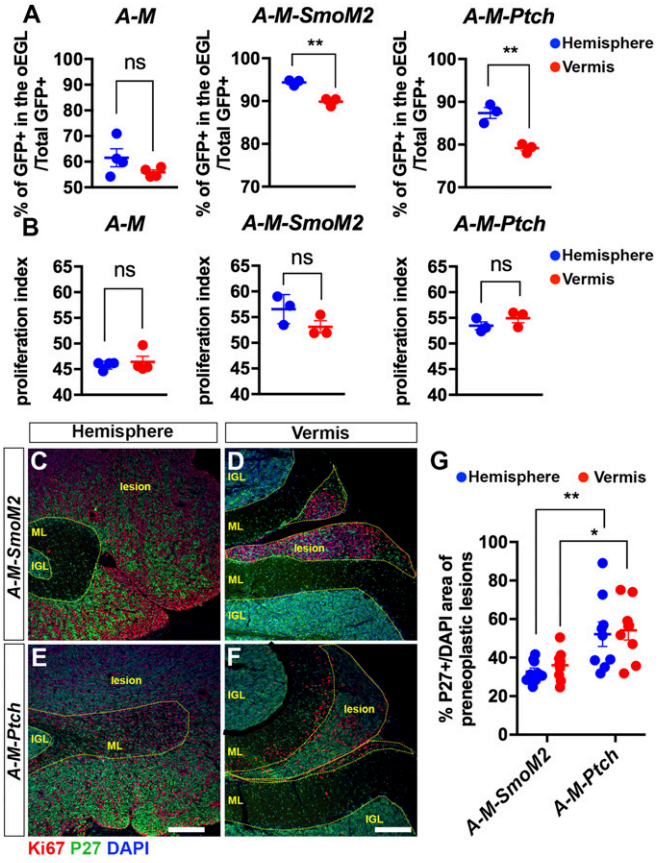

Fig. 3. GCPs located in the hemispheres are more sensitive to elevated HH signaling, which maintains them in an undifferentiated state. (*A* and *B*) Graphs of the proportions of undifferentiated GCPs (GFP^+ in the proliferating outer EGL/total GFP^+ cells) (*A*) and the proliferation index (percent GFP^+ EdU^+ cells/GFP^+ in outer EGL) (*B*) in H and V of P8 *A-M* ($n = 4$), *A-M-SmoM2* ($n = 3$), and *A-M-Ptch* ($n = 3$) mice. Significances determined using paired Student's *t* test to compare H and V within an animal of each genotype. (*C*–*F*) Flourescent immunohistochemical (FIHC) detection of K_i67, P27, and DAPI on sagittal sections of P21 *A-M-SmoM2* and *A-M-Ptch* mice. Internal granule cell layer (IGL), molecular layer (ML), and lesions are indicated with yellow dotted lines. (Scale bars, 200 μm.) (*G*) Quantification of cell differentiation ($P27^+$ over $DAPI^+$ area) in preneoplastic lesions located in H and V of P21 *A-M-SmoM2* ($n = 3$) and *A-M-Ptch* ($n = 3$) mice. Significances determined using two-way ANOVA (overall $P = 0.0001$) followed by a Sidak post hoc test. All data are expressed as mean ± SEM. $^{**}P < 0.01$, $^{*}P < 0.05$, ns, nonsignificant. Statistics are provided in Table S2.

***SmoM2*-Mutant GCPs from the H Show Increased Tumorigenicity.** Because the GCPs in the H are more sensitive to high SHH signaling compared with those in the V, and tumors only form in the H of *A-SmoM2* mice, we asked whether *SmoM2*-mutant GCPs in the H also have greater potential to form tumors. We isolated *SmoM2*-mutant GCPs at P8 from the H (P8 SmoM2-H) or V (P8 SmoM2-V) by the Percoll gradient method and injected 5×10^5 cells into the right H of nude mice (Fig. 4*A*). Mice transplanted with P8 SmoM2-H GCPs died significantly earlier than those injected with P8 SmoM2-V GCPs (median survival: H vs. V = 42 d vs. 72.5 d; 9 of 10 vs. 6 of 10 mice died by 90 d). We then performed transplantation of *SmoM2*-mutant cells isolated at P21, an early stage of tumor progression (Fig. 4*B*). Interestingly, only mice transplanted with P21 SmoM2-H cells showed signs of tumor burden by 90 d ($n = 7$ of 10 P21 SmoM2-H mice, median survival of 55 d and $n = 0$ of 10 for P21 SmoM2-V). The tumor histology of P8 SmoM2-H, P8 SmoM2-V and P21 SmoM2-H resembled that of the *A-SmoM2* tumors (Fig. S7). In conclusion, *SmoM2*-mutant GCPs from the H are more tumorigenic after transplantation than those from the V.

To directly test whether *SmoM2*-mutant GCPs from the V have low tumorigenic potential, we utilized a V-specific Tm-inducible *Cre* line to induce SmoM2 expression only in V GCPs ($En1^{CreER/+}$; $R26^{LSL\text{-}SmoM2\text{-}YFP/+}$ mice) (23). As expected, at P21, we observed preneoplastic lesions with proliferating cells only in the V ($n = 5$) (Fig. 4*C*). However, none of the mice developed tumors by 3 mo of age ($n = 9$ of 10 mice had no proliferating lesions and 1 of 10 mice had a small lesion in the V) (Fig. 4*D*), providing further proof that V GCPs are not sensitive to tumor formation by SmoM2 after birth.

GCPs in the H and V Exhibit Differential Gene-Expression Profiles. We next performed a microarray analysis to identify location-specific genes that influence GCP behaviors. GCPs from WT and *A-SmoM2* mice given a high dose of Tm at P2 were isolated from the H or V using a Percoll gradient. Twenty-eight genes were found to be differentially expressed (>twofold with a false-discovery rate of $P = 0.05$) in GCPs from the H compared with V of WT mice and 17 genes from *A-SmoM2* mutants (Fig. S8A). To focus on genes that generally predispose GCPs to malignant transformation, we chose the five genes (*En1*, *1500015O10Rik*, *Ccsc153*, *EphA3*, *Nr2f2*) that were differentially expressed between the two locations in WT and *SmoM2*-mutant GCPs. Three of five shared genes had a similar expression tendency using qRT-PCR of GFP^+ GCPs isolated from the cerebellum of P8 *Atoh1-GFP*/+ mice (Fig. S8B). RNA in situ hybridization analysis of the three differentially expressed genes showed clear regionally restricted expression, with *Nr2f2* and *EphA3* expression in the EGL restricted to the H and *En1*, as expected (23, 24), to the V in both WT and *SmoM2*-mutant GCPs (Fig. 5 *A* and *B* and Fig. S9 A–D). For *Nr2f2* and *En1*, the location differences were maintained in *Atoh1-SmoM2* P21 lesions (Fig. 5 *C* and *D*), as well as *A-M-Ptch* lesions (Fig. S9 E and F), and *Nr2f2* continued to be expressed, although at a lower level, in tumors of both models (Figs. S8B and S9 G and H). NR2F2 (COUP-TFII) is a transcription factor that plays important roles in multiple developmental processes (25, 26) and a high level of NR2F2 is associated with tumor angiogenesis, invasion, and metastasis (27, 28). However, the role of NR2F2 has not been studied in MB. We therefore analyzed *NR2F2* expression in human MB samples and found higher expression in MBs compared with the normal adult cerebellum, and interestingly *NR2F2* was

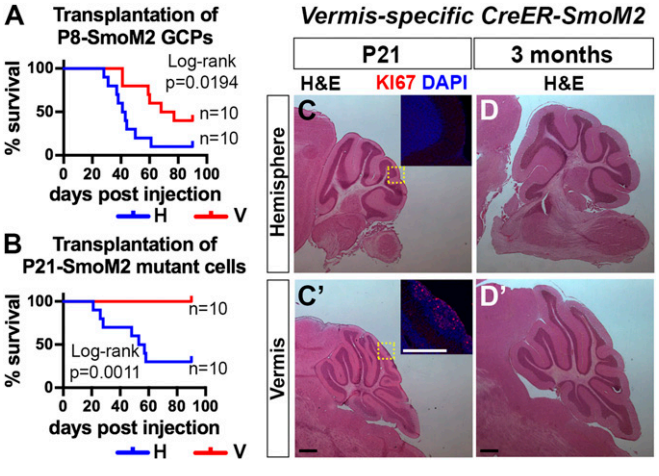

Fig. 4. *SmoM2*-mutant cells in the H show higher tumor-initiating potential compared with in the V. (*A* and *B*) Survival curves of nude mice transplanted with *SmoM2*-mutant GCPs or preneoplastic cells isolated at P8 (*A*) or P21 (*B*) from the H or V of *A-SmoM2* mice. Ninety days postinjection was the experimental endpoint. (*C*) H&E staining of sagittal H (*C*) and V (*C′*) sections from P21 V-specific *CreER-SmoM2* ($En1^{CreER/+}$) mice given Tm at P2. FIHC detection of K_i67 and DAPI in areas indicated by yellow rectangles in *C* and *C′*. (*D*) H&E staining of sagittal H (*D*) and V (*D′*) sections of 3-mo-old V-specific *CreER-SmoM2* mice. (Scale bars, 500 μm.)

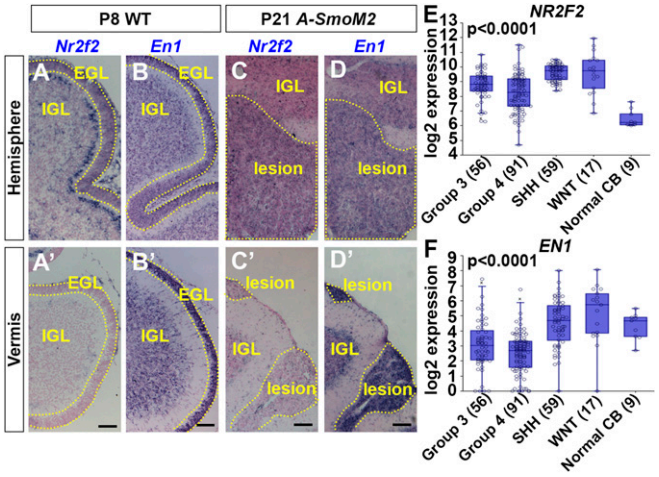

Fig. 5. GCP location-specific gene expression in lesions and tumors. (*A–D*) RNA in situ hybridization of *Nr2f2* (*A* and *C*) and *En1* (*B* and *D*) on the sagittal section of H and V (*A′–D′*) from P8 WT (*A* and *B*) and P21 *A-SmoM2* (*C* and *D*) mice. IGL, EGL, and lesion are marked by dotted lines. (Scale bars, 75 μm.) (*E* and *F*) Expression of *NR2F2* (*E*) and *EN1* (*F*) in four subgroups of human MB [R2: Genomics Analysis and Visualization Platform (https://hgserver1.amc.nl/cgi-bin/r2/main.cgi)]; significance is calculated with a one-way ANOVA between groups.

highest in the SHH and WNT subgroups (Fig. 5*E*). In a second cohort of MB, *NR2F2* was also found to be high in all four subtypes of SHH-MB (Fig. S9I). EN1 is a homeobox-containing transcription factor that plays multiple roles in cerebellum development (29, 30). The expression of *EN1* was found to be low across all four subgroups of MBs (Fig. 5*F* and Fig. S9J).

***Nr2f2* Promotes an Undifferentiated State and *En1/2* a Differentiated State in *SmoM2*-Mutant GCPs.** We next tested whether, given their distinct locations in the cerebellum, *Nr2f2* and *En1* play different roles in differentiation of *SmoM2*-mutant GCPs using our MASTR approach. Because *En1* has overlapping functions with *En2* in the cerebellum (29–31), both genes were ablated. *A-M-SmoM2;Nr2f2*$^{flox/flox}$ (*A-M-SmoM2-N*), *A-M-SmoM2;Nr2f2*$^{flox/+}$ (*A-M-SmoM2-N* het), and *A-M-SmoM2;En1*$^{flox/flox}$*;En2*$^{flox/flox}$ (*A-M-SmoM2-E*) mice were given Tm at P2 and the percentages of undifferentiated GFP^{+} GCPs were quantified at P8. Strikingly, loss of either one or two copies of *Nr2f2* led to a decrease in the proportion of undifferentiated *SmoM2*-mutant GCPs in the H compared with *A-M-SmoM2* controls (Figs. 3*A* and 6*A*). Consistent with *Nr2f2* being expressed specifically in H GCPs, the percentage of undifferentiated cells did not change in the V between *Nr2f2*-mutants and controls (Fig. 6*A*). In contrast, loss of *En1/2* led to an increase in the percentage of *SmoM2*-mutant GCPs in the V compared with *A-M-SmoM2* controls (Fig. 6*B*). These results suggest that *Nr2f2* plays a role in maintaining *SmoM2*-mutant GCPs in a progenitor state in the H, whereas *En1/2* promotes differentiation in the V.

To test whether these genes have a major functional role in SHH-MB formation, we analyzed *A-M-SmoM2-N* and *-E* mice at P45. Although loss of *Nr2f2* led to slightly more differentiation of *SmoM2*-mutant cells in the H at P8, the average size of H lesions at P45 was not reduced compared with *A-M-SmoM2* controls (Fig. 6*C* and Fig. S10 A–D). Whereas loss of *En1/2* slightly increases the proportion of undifferentiated *SmoM2*-mutant cells in the V at P8, we only observed a lesion in the V of 1/7 *A-M-SmoM2-E* mice at P45 (Fig. S10E). Thus, while *Nr2f2* and the *En* genes modulate the effect of SmoM2 on GCP differentiation, they are not necessary for, or sufficient to induce tumors.

Discussion

The presentation, genetics, and outcomes of SHH-MB differ between adults and other age groups, raising the question of whether the etiology of adult SHH-MB is distinct (2, 32). Using sporadic mouse models with the two HH-activating mutations seen most commonly in adult SHH-MB (2, 13), we uncovered that all *SmoM2*-mutant and most *Ptch1*-mutant tumors form in the H. Moreover, inducing the *SmoM2* mutation specifically in V GCPs did not lead to tumor formation. Using transplantation analysis, we found that the susceptibility of the H to tumor formation is present as early as P8. Strikingly, inducing SmoM2-expression in GCPs in the embryo (E14.5) did not alter tumor location. Our results thus show that for *SmoM2*-mutant GCPs to form tumors, those in the V must accumulate additional mutations not necessary in hemispheric GCPs, providing one reason why adult SHH-MBs where *SMO* mutations are prevalent are located in the H more often than in younger ages.

Our study shows that GCPs can be divided into distinct populations based on location-specific characteristics, including molecular profiles and cell behaviors. Others have proposed that GCPs have specific gene-expression profiles related to the functional circuits they participate in (33), and a subset of GCPs from the P7 cerebellum were shown to express the stem cell marker Prominin (34). Here, we highlight the diversity of these cells by demonstrating that only a subset of GCPs is capable of generating SHH-MBs. Likely partially accounting for this, GCPs in the H with elevated HH signaling are preferentially maintained in an undifferentiated state compared with the V. Furthermore, our mosaic analysis revealed that the two top location-specific genes (*En1* and *Nr2f2*) have an impact on *SmoM2*-mutant GCP differentiation. The hemisphere-specific gene *Nr2f2* is particularly interesting because it contributes to maintaining GCPs with activated SHH signaling in an undifferentiated state. However, unlike its oncogenic functions in other tissues (35, 36), we found that *Nr2f2* is not required for SHH-MB initiation, indicating that additional genes can compensate for loss of *Nr2f2*. Interestingly, using longitudinal MRI imaging of *A-SmoM2* mice, we uncovered that tumors not only arise from the H, but more specifically, from the posterior/ventral region of the lateral cerebellum. This posterior/ventral location of SHH-MB has not been noted previously, and was observed at P21 and later stages in our models. The specificity of the location within the H potentially explains why

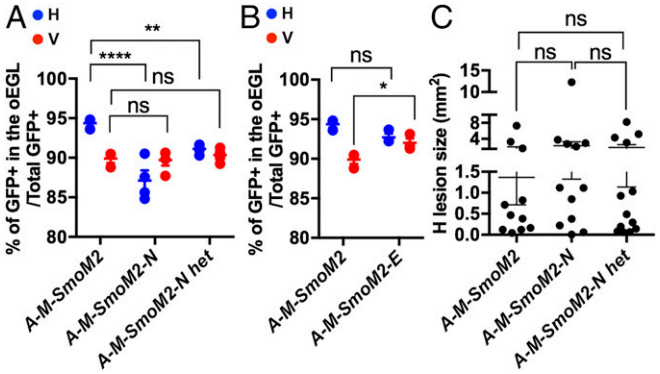

Fig. 6. *Nr2f2* and *En1/2* influence the differentiation of *SmoM2*-mutant P8 GCPs but not tumor formation. (*A*) Graphs comparing the proportions of undifferentiated GCPs between H and V of *A-M-SmoM2* (also shown in Fig. 3*A*), *A-M-SmoM2-N* ($n = 4$), and *A-M-SmoM2-N* het ($n = 5$) mice. (*B*) Graphs comparing the proportions of undifferentiated GCPs between the H and V of *A-M-SmoM2* and *A-M-SmoM2-E* ($n = 3$) mice. (*C*) Graphs showing the size of H lesions from *A-M-SmoM2* ($n = 11$), *A-M-SmoM2-N* ($n = 12$), and *A-M-SmoM2-N* het ($n = 13$). Significances determined using a two-way ANOVA followed by a Sidak post hoc test for *A* and *B*, or with a one-way ANOVA followed by Tukey post hoc test for *C*. All data are expressed as mean ± SEM. ****$P < 0.0001$, **$P < 0.01$, *$P < 0.05$, ns, nonsignificant. Statistics are provided in Table S2.

Nr2f2 alone is not necessary for *A-M-SmoM2* mice to form tumors because it is expressed throughout the H. A recent paper suggested that mutations in genes related to the TP53 pathway are required for mutant GCPs in *Ptch1*$^{+/-}$ mice to evade cell senescence in preneoplastic lesions to form tumors (37), raising the question of whether GCPs located in the posterior/ventral H are more susceptible to secondary mutations that cause senescence evasion. It is likely that SHH-MBs preferentially develop in the posterior/ventral H due to a combination of spatially restricted intrinsic factors, additional mutations, and potentially different environmental cues.

Our study provides experimental evidence that the type of activating mutation modulates tumor biology. Interestingly, we found in humans that different HH-pathway activating driver mutations and to a lesser degree the age of tumor presentation appear to influence tumor location. Although *SUFU* mutations are rare and mainly occur in the infant age group (3), the two infant *SUFU*-mutant MB samples we analyzed were located in the V. Notably, in the five samples with a *SMO* mutation, all four adult tumors were located in the H and the one infant tumor was located in the V. In contrast, tumors with a *PTCH1* mutation were preferentially located in the H for both infant and adult patients (five of seven in infant and five of nine in adult). Consistent with the human data, in our mouse models, activating HH signaling through two different mutations resulted in differences in GCP behavior and tumor biology, as *SmoM2* maintains mutant GCPs in an undifferentiated state to a greater extent than loss-of-*Ptch1* at both P8 and P21. Compensation by *Ptch2* for loss-of *Ptch1* might contribute to the milder phenotype compared with expression of *SmoM2* (38). Moreover, because differentiated neurons have been shown to secrete cytokines that promote growth in SHH-MB and other cancers (39, 40), perhaps the higher differentiation seen in *A-M-Ptch* mice accounts for some tumors forming in the V. In addition, each type of mutation could interact distinctly with location-specific properties of GCPs, thus resulting in different tumor progression profiles.

In summary, our study demonstrates that SHH-MBs driven by either *SmoM2* or loss-of-*Ptch1* mutations have different tumor biology. Furthermore, GCPs are heterogeneous and their response to activated HH signaling is dictated by the type of mutation and the cell location. Our findings provide experimental evidence in mouse models that SHH-MB is not a single disease, and emphasize the need for further research to decipher the full extent of diversity of GCPs and their impact on MB tumorigenesis.

Materials and Methods

All animal experiments were performed with the approval of the Institutional Animal Care and Use Committees at Memorial Sloan Kettering Cancer Center and the New York University School of Medicine. Details of experimental methods and statistical analyses are included in *SI Materials and Methods*. Significance was determined as $P < 0.05$.

ACKNOWLEDGMENTS. We thank past and present members of the A.L.J. laboratory for discussions and technical help; Elyn Riedel for consultation on statistical approaches; and Synphen Wu for comments on the manuscript. This work was supported by NIH Grants R01CA192176 and R37MH085726 (to A.L.J.); the National Brain Tumor Society (A.L.J.); Memorial Sloan Kettering Cancer Center (MSKCC) Geoffrey Beene Cancer Research Center Grant 21680 (to A.L.J.); MSKCC Brain Tumor Center and Philippe Foundation (A.W.); and National Cancer Institute Cancer Center Support Grant P30 CA008748-48.

1. Northcott PA, Korshunov A, Pfister SM, Taylor MD (2012) The clinical implications of medulloblastoma subgroups. *Nat Rev Neurol* 8:340–351.
2. Kool M, et al.; ICGC PedBrain Tumor Project (2014) Genome sequencing of SHH medulloblastoma predicts genotype-related response to smoothened inhibition. *Cancer Cell* 25:393–405.
3. Louis DN, et al. (2016) The 2016 World Health Organization classification of tumors of the central nervous system: A summary. *Acta Neuropathol* 131:803–820.
4. Northcott PA, et al. (2017) The whole-genome landscape of medulloblastoma subtypes. *Nature* 547:311–317.
5. Cavalli FMG, et al. (2017) Intertumoral heterogeneity within medulloblastoma subgroups. *Cancer Cell* 31:737–754.e6.
6. Thompson EM, et al. (2016) Prognostic value of medulloblastoma extent of resection after accounting for molecular subgroup: A retrospective integrated clinical and molecular analysis. *Lancet Oncol* 17:484–495.
7. Corrales JD, Blaess S, Mahoney EM, Joyner AL (2006) The level of sonic hedgehog signaling regulates the complexity of cerebellar foliation. *Development* 133: 1811–1821.
8. Dobbing J, Sands J (1973) Quantitative growth and development of human brain. *Arch Dis Child* 48:757–767.
9. Rakic P, Sidman RL (1970) Histogenesis of cortical layers in human cerebellum, particularly the lamina dissecans. *J Comp Neurol* 139:473–500.
10. Leto K, et al. (2016) Consensus paper: Cerebellar development. *Cerebellum* 15: 789–828.
11. Yang ZJ, et al. (2008) Medulloblastoma can be initiated by deletion of patched in lineage-restricted progenitors or stem cells. *Cancer Cell* 14:135–145.
12. Schüller U, et al. (2008) Acquisition of granule neuron precursor identity is a critical determinant of progenitor cell competence to form Shh-induced medulloblastoma. *Cancer Cell* 14:123–134.
13. Pöschl J, et al. (2014) Genomic and transcriptomic analyses match medulloblastoma mouse models to their human counterparts. *Acta Neuropathol* 128:123–136.
14. Remke M, et al. (2013) TERT promoter mutations are highly recurrent in SHH subgroup medulloblastoma. *Acta Neuropathol* 126:917–929.
15. Wefers AK, et al. (2014) Subgroup-specific localization of human medulloblastoma based on pre-operative MRI. *Acta Neuropathol* 127:931–933.
16. Perreault S, et al. (2014) MRI surrogates for molecular subgroups of medulloblastoma. *AJNR Am J Neuroradiol* 35:1263–1269.
17. Zhao F, et al. (2017) Distinctive localization and MRI features correlate of molecular subgroups in adult medulloblastoma. *J Neurooncol* 135:353–360.
18. Ohli J, Neumann JE, Grammel D, Schüller U (2015) Localization of SHH medulloblastoma in mice depends on the age at its initiation. *Acta Neuropathol* 130:307–309.
19. Mao J, et al. (2006) A novel somatic mouse model to survey tumorigenic potential applied to the Hedgehog pathway. *Cancer Res* 66:10171–10178.
20. Ellis T, et al. (2003) Patched 1 conditional null allele in mice. *Genesis* 36:158–161.
21. Lao Z, Raju GP, Bai CB, Joyner AL (2012) MASTR: A technique for mosaic mutant analysis with spatial and temporal control of recombination using conditional floxed alleles in mice. *Cell Reports* 2:386–396.
22. Suero-Abreu GA, et al. (2014) In vivo Mn-enhanced MRI for early tumor detection and growth rate analysis in a mouse medulloblastoma model. *Neoplasia* 16:993–1006.
23. Sgaier SK, et al. (2005) Morphogenetic and cellular movements that shape the mouse cerebellum; insights from genetic fate mapping. *Neuron* 45:27–40.
24. Wilson SL, Kalinovsky A, Orvis GD, Joyner AL (2011) Spatially restricted and developmentally dynamic expression of engrailed genes in multiple cerebellar cell types. *Cerebellum* 10:356–372.
25. Naka H, Nakamura S, Shimazaki T, Okano H (2008) Requirement for COUP-TFI and II in the temporal specification of neural stem cells in CNS development. *Nat Neurosci* 11: 1014–1023.
26. Srinivasan RS, et al. (2010) The nuclear hormone receptor Coup-TFII is required for the initiation and early maintenance of Prox1 expression in lymphatic endothelial cells. *Genes Dev* 24:696–707.
27. Qin J, et al. (2013) COUP-TFII inhibits TGF-β-induced growth barrier to promote prostate tumorigenesis. *Nature* 493:236–240.
28. Polvani S, et al. (2014) COUP-TFII in pancreatic adenocarcinoma: Clinical implication for patient survival and tumor progression. *Int J Cancer* 134:1648–1658.
29. Sgaier SK, et al. (2007) Genetic subdivision of the tectum and cerebellum into functionally related regions based on differential sensitivity to engrailed proteins. *Development* 134:2325–2335.
30. Orvis GD, et al. (2012) The engrailed homeobox genes are required in multiple cell lineages to coordinate sequential formation of fissures and growth of the cerebellum. *Dev Biol* 367:25–39.
31. Cheng Y, et al. (2010) The engrailed homeobox genes determine the different foliation patterns in the vermis and hemispheres of the mammalian cerebellum. *Development* 137:519–529.
32. Northcott PAHT, et al. (2011) Pediatric and adult sonic hedgehog medulloblastomas are clinically and molecularly distinct. *Acta Neuropathol* 122:231–240.
33. Hatten ME, Roussel MF (2011) Development and cancer of the cerebellum. *Trends Neurosci* 34:134–142.
34. Sutter R, et al. (2010) Cerebellar stem cells act as medulloblastoma-initiating cells in a mouse model and a neural stem cell signature characterizes a subset of human medulloblastomas. *Oncogene* 29:1845–1856.
35. Nagasaki S, et al. (2009) Chicken ovalbumin upstream promoter transcription factor II in human breast carcinoma: Possible regulator of lymphangiogenesis via vascular endothelial growth factor-C expression. *Cancer Sci* 100:639–645.
36. Navab R, et al. (2004) Expression of chicken ovalbumin upstream promoter-transcription factor II enhances invasiveness of human lung carcinoma cells. *Cancer Res* 64: 5097–5105.
37. Tamayo-Orrego L, et al. (2016) Evasion of cell senescence leads to medulloblastoma progression. *Cell Rep* 14:2925–2937.
38. Lee Y, et al. (2006) Patched2 modulates tumorigenesis in patched1 heterozygous mice. *Cancer Res* 66:6964–6971.
39. Snuderl M, et al. (2013) Targeting placental growth factor/neuropilin 1 pathway inhibits growth and spread of medulloblastoma. *Cell* 152:1065–1076.
40. Venkatesh H, Monje M (2017) Neuronal activity in ontogeny and oncology. *Trends Cancer* 3:89–112.